More accuracy approach for signal subspace-based algorithms in bistatic EMVS-MIMO radar

Fengtao Xue
National University of Defense Technology
Yunxiu Yang
South-West Institute of Technical Physics
Maoyuan Feng
1170475472@qq.com

Sichuan University
Qin Shu
Sichuan University

Research Article

Keywords: Angle estimaion, MIMO radar, Electromagnetic vector sensors.

Posted Date: September 14th, 2023

DOI: https://doi.org/10.21203/rs.3.rs-3339610/v1

Additional Declarations: No competing interests reported.

Version of Record: A version of this preprint was published at Signal, Image and Video Processing on February 26th, 2024. See the published version at https://doi.org/10.1007/s11760-024-03041-3.

More accuracy approach for signal subspace-based algorithms in bistatic EMVS-MIMO radar

Fengtao Xue[a], Yunxiu Yang[b], Maoyuan Feng[c,*], Qin Shu[c]

[a]*410003 National University of Defense Technology, Changsha, China*
[b]*610041 South-West Institute of Technical Physics, Chengdu, China*
[c]*610065 College of Electrical Engineering, Sichuan University, Chengdu, China*

Abstract

In this article, we rediscuss the parameter estimation in a bistatic multiple-input multiple-output radar system with electromagnetic vector sensor (EMVS) and propose an improved approach for all signal subspace-based estimation algorithms. First, the signal subspace is obtained by directly performing SVD or high-order SVD on the signal matrix or the signal tensor. Then, the elevation angle is automatically estimated by exploiting the rotation invariance of the receive-transmit array manifold and the Joint diagonalization technology. Then, the estimated elevation angle is taken as prior information, and the spatial response vector is recovered from the entire signal subspace using least-squares by exploring the property of the Kronecker product. Next, the azimuth angle is estimated by the 'Vector Cross-Product' strategy. Finally, the polarization parameters are calculated based on the least-squares method. The proposed algorithm is analyzed from the aspects of identifiability and complexity. The proposed signal subspace acquisition method is less computationally intensive. The improved parameter estimation approach can realize automatic parameter pairing and have a better parameter estimation performance than the previous corresponding algorithms when it works on the subspace obtained in different ways. Simulation results verify the performance improvement of the proposed algorithm.

Keywords: Angle estimaion, MIMO radar, Electromagnetic vector sensors.

*Corresponding author
Email address: 1170475472@qq.com (Maoyuan Feng)

1. Introduction

Multiple-input multiple-output is an emerging direction estimation technology in radar systems since it has unique advantages and outstanding performance compared to the traditional phased array radar system [1, 2, 3]. The estimation of the direction-of-departure (DOD) and direction-of-arrival (DOA) has been extensively studied for multiple-input multiple-output radar [4, 5, 6, 7, 8]. However, the number of literature studied on two-dimensional (2D) problems, namely azimuth, and elevation, 2D-DOD, and 2D-DOA estimation, is limited [9, 10, 11]. Chen and Zhang developed a PM-based algorithm for 2D-DOD and 2D-DOA estimation algorithm in MIMO radar with arbitrary arrays[9]. An improved ESPRIT-bassed algorithm was introduced for 2D-DOD, and 2D-DOA estimation in MIMO radar with arbitrary arrays [10]. In [11], a new approach that combines ESPRIT and joint diagonalization technology was proposed for 2D-DOD and 2D-DOA estimation in bistatic MIMO radar with an L-shaped array. These methods developed for 2D-DOD and 2D-DOA estimation are based on scalar sensors. A typical character of [9, 10, 11] is that the antenna array is nonlinear, e.g., L-shape, rectangular, or arbitrary shape. As an alternative to the scalar sensor, the electromagnetic vector sensor (EMVS) brings new development space for target positioning [12]. The EMVS at a certain point in space can provide a 2D direction finding [13]. Besides, it can also provide the polarization state of the input signal, which provides new potential possibilities for detecting invisible targets.

The use of EMVS for direction finding has become a hot research topic, and various estimators have been proposed in [12, 13, 14, 15, 16]. A general bistatic MIMO-EMVS radar with multiple transmit and receive EMVSs was introduced in [17], and a ESPRIT-like algorithm was proposed to estimate 2D-DOD, 2D-DOA, 2D transmit polarization angle (TPA) and 2D receive polarization angle(RPA). First, the signal subspace is obtained by performing eigen decomposition (EVD) on the covariance matrix of the received data. Next, a rotation matrix is obtained from the 6N/6M rows of the signal subspace by exploiting the rotation invariance of the receive/transmit array manifold and use it to recover the receive/transmit spatial response vector from these rows where N/M is the number of receive/transmit arrays. The 2D-DOA and 2D-DOD are estimated via 'Vector Cross-Product' idea using the recovered spatial response vector. Then, the 2D-TPA and 2D-RPA are estimated by least-squares method. Finally, the orthogonality of the virtual

steering vector and the noise subspace is used to the pairing of the transmit and receive parameters. In [18], the signal subspace is obtained by directly performing high-order SVD on the covariance tensor, then all parameters are estimated by using the same process as that in [17]. The HOSVD based algorithm can improve the signal subspace estimation accuracy to improve the parameter estimation performance, but it suffers a high computational complexity. To avoid decomposition, the signal subspace is obtained by the propagator method in [19]. Then, all parameters are estimated by using the same process in [17], except the elevation angle is estimated from the rotation matrix. The above algorithms only select 6N/6M rows of the signal subspace to estimate all parameters and do not fully utilize the entire signal subspace. Furthermore, in [20], by exploiting the rotation invariance of the virtual array manifold, the elevation angle is estimated from the entire signal subspace obtained by PM. However, other parameters estimation process is the same as that in [17], except no need for the other pairing process. It is a pity that only the elevation angle estimation make full use of the entire signal subspace. We can know that all algorithms based on signal subspace do not make full use of the entire signal subspace to estimate all parameters through the above introduction. They only select 6N/6M rows of the signal subspace to estimate the parameter and waste most of the signal subspace, which will cause performance degradation. Besides, as shown in [17], parameter estimation accuracy is also affected by the position of the selected part in the signal subspace. Different positions of the selected part in the signal subspace will bring different estimation results. So it is difficult to determine which part can get the best estimation effect. All the algorithms mentioned above, except HOSVD, do not make full use of the inherent multi-dimensional structure of the matched filters, resulting in some performance loss. The authors in [21] make full use of the inherent multi-dimensional structure, and introduce the trilinear decomposition to obtain the estimation of the loading matrices, and use those loading matrices to realize the separate estimate of the receive and transmit parameters. At the same time, the transmit and receive parameters are automatically paired.

In this paper, we introduce two effective ways to get signal subspace and propose an improved approach suitable for all signal subspace-based algorithms in bistatic EMVS-MIMO radar parameter estimation to save computational load and make full use of the entire signal subspace in the bistatic EMVS-MIMO radar. The main contributions of this paper are as follows: (1)Two effective ways to obtain the signal subspace are introduced to re-

duce the computational complexity, namely, directly performing singular value decomposition (SVD) on the data matrix or performing high-order SVD (HOSVD) on the data tensor to get the signal subspace. (2) To make full use of the virtual array manifold of the MIMO radar and the entire signal subspace, an improved approach suitable for all signal subspace-based algorithms is proposed. The transmit/receive parameters do not affect the receive/transmit parameters estimation is proved. (3) The computational complexity and the number of identifiable targets of the proposed algorithm are analyzed and compared with the existing algorithms. Numerical simulations are further used to verify the effectiveness of the proposed algorithm. What needs special emphasis is that although in the new parameter estimation approach, it combines the ESPRIT and "Vector Cross-Product" ideas to estimate the parameters, the difference from the existing algorithms are: (1) The transmit/receive elevation angle is estimated by exploiting the rotation invariance of the virtual array manifold of the MIMO radar, instead of the transmit/receive array manifold. The joint diagonalization technology is introduced to ensures the pairing estimation of the receive and transmit elevation angle, and no additional pairing process is required. (2) The transmit/receive spatial response vector is recovered from the $36NM$ rows of the signal subspace, instead of the $6M/6N$ rows of the signal subspace. As above, all parameters estimation are obtained from the whole signal subspace instead of the 6M or 6N rows of the signal subspace. Therefore, when the improved approach is applied to the signal subspace obtained by different ways, a certain degree of performance improvement will be obtained compared with the original parameter estimation method.

The rest of this paper is organized as follows: The signal model for bistatic EMVS-MIMO radar is introduced in section 2, the signal subsapce obtain by perform SVD on the data matrix and perform HOSVD on the data tensor are presented in section 3, the improved signal subspace-based parameter estimation approach is introduced in section 4. The performance including identifiability, complexity, and CRB are derived in section 5. Several numerical results are provided to indicate the effectiveness of the proposed algorithm in section 6. Finally, a conclusion is drawn in section 7.

Notation : We use symbols $(\bullet)^{\mathrm{T}}$, $(\bullet)^{\mathrm{H}}$, $(\bullet)^{-1}$ and $(\bullet)^{*}$ to represent transposition operator, conjugate transposition operator, matrix inverse operator and conjugate operator, respectively. $\oplus$, $\odot$ and $\otimes$ represent the Hadamard product, Khatri-Rao product and Kronecker product, respectively. vec$\{\bullet\}$ denotes straightening the matrix $\mathbf{A} \in \mathbb{C}^{N\times M}$ into a column vector $\mathbf{a} \in \mathbb{C}^{MN\times 1}$,

in which $\mathbf{a}_{(m-1)N+n} = \mathbf{A}_{n,m}$. angle$\{a\}$ stands for the phase of a; The 'Vector Cross-Product' between $\mathbf{a}_1 = [a_1,\, a_2,\, a_3]^{\mathrm{T}}$ and $\mathbf{a}_2 = [a_4,\, a_5,\, a_6]^{\mathrm{T}}$ is defined as $\mathbf{a}_1 \circledast \mathbf{a}_2 = \begin{bmatrix} 0 & -a_3 & a_2 \\ a_3 & 0 & -a_1 \\ -a_2 & a_1 & 0 \end{bmatrix} \begin{bmatrix} a_4 \\ a_5 \\ a_6 \end{bmatrix}$.

2. Signal model

Consider the same bistatic EMVS-MIMO radar system scenario to that in Chintagunta and Palanisamy [17], which is equiped with an M-element EMVS transmit arrays and an N-element EMVS receive arrays. Both of them are uniform linear array (ULA). Suppose there are K far-field point-like targets located at the same range bin. The 2D-DOD pair and 2D-DOA pair of the kth target are $(\theta_{t,k}, \phi_{t,k})$ and $(\theta_{r,k}, \phi_{r,k})$, respectively, where $\theta_{t,k}$, $\theta_{r,k}$ are the elevation angles, $\phi_{t,k}$, $\phi_{r,k}$ are the azimuth angles. The transmit and the receive steering vector of the k-th target can be expressed as [17]

$$\mathbf{b}_{t,k} = \mathbf{a}_{t,k} \otimes \mathbf{c}_{t,k} \tag{1a}$$

$$\mathbf{b}_{r,k} = \mathbf{a}_{r,k} \otimes \mathbf{c}_{r,k} \tag{1b}$$

where $\mathbf{a}_{t,k} = [1, e^{j2\pi d_t \sin(\theta_{t,k})/\lambda}, \cdots, e^{j2\pi(M-1)d_t \sin(\theta_{t,k})/\lambda}]^{\mathrm{T}} \in \mathbb{C}^{M\times 1}$ and $\mathbf{a}_{r,k} = [1, e^{j2\pi d_r \sin(\theta_{r,k})/\lambda}, \cdots, e^{j2\pi(N-1)d_r \sin(\theta_{r,k})/\lambda}]^{\mathrm{T}} \in \mathbb{C}^{N\times 1}$ in which λ, d_t, d_r are the wavelength, the spacing of adjacent transmit array, the spacing of adjacent receive array, respectively, $\mathbf{c}_{t,k}/\mathbf{c}_{r,k}$ stands for the spatial response of an EVS associated with the transmitter/receiver. Moreever, $\mathbf{c}_{t,k}$ and $\mathbf{c}_{r,k}$ can be expressed in detail as

$$\mathbf{c}_{t,k} = \mathbf{F}_{t,k}\mathbf{h}_{t,k} = \left[\underbrace{c_{t_1,k}, c_{t_2,k}, c_{t_3,k}}_{\mathbf{c}_{t_1,k}^{\mathrm{T}}}, \underbrace{c_{t_4,k}, c_{t_5,k}, c_{t_6,k}}_{\mathbf{c}_{t_2,k}^{\mathrm{T}}} \right]^{\mathrm{T}}, \tag{2a}$$

$$\mathbf{c}_{r,k} = \mathbf{F}_{r,k}\mathbf{h}_{r,k} = \left[\underbrace{c_{r_1,k}, c_{r_2,k}, c_{r_3,k}}_{\mathbf{c}_{r_1,k}^{\mathrm{T}}}, \underbrace{c_{r_4,k}, c_{r_5,k}, c_{r_6,k}}_{\mathbf{c}_{r_2,k}^{\mathrm{T}}} \right]^{\mathrm{T}}, \tag{2b}$$

in which

$$\mathbf{F}_{t,k} = \begin{bmatrix} \cos(\phi_{t,k})\cos(\theta_{t,k}) & -\sin(\phi_{t,k}) \\ \sin(\phi_{t,k})\cos(\theta_{t,k}) & -\cos(\phi_{t,k}) \\ -\sin(\theta_{t,k}) & 0 \\ -\sin(\phi_{t,k}) & -\cos(\phi_{t,k})\cos(\theta_{t,k}) \\ \cos(\phi_{t,k}) & -\sin(\phi_{t,k})\cos(\theta_{t,k}) \\ 0 & \sin(\theta_{t,k}) \end{bmatrix} \tag{3a}$$

$$\mathbf{F}_{r,k} = \begin{bmatrix} \cos(\phi_{r,k})\cos(\theta_{r,k}) & -\sin(\phi_{r,k}) \\ \sin(\phi_{r,k})\cos(\theta_{r,k}) & -\cos(\phi_{r,k}) \\ -\sin(\theta_{r,k}) & 0 \\ -\sin(\phi_{r,k}) & -\cos(\phi_{r,k})\cos(\theta_{r,k}) \\ \cos(\phi_{r,k}) & -\sin(\phi_{r,k})\cos(\theta_{r,k}) \\ 0 & \sin(\theta_{r,k}) \end{bmatrix} \tag{3b}$$

and

$$\mathbf{h}_{t,k} = \begin{bmatrix} \sin(\gamma_{t,k})e^{j\eta_{t,k}} \\ \cos(\gamma_{t,k}) \end{bmatrix} \tag{4a}$$

$$\mathbf{h}_{r,k} = \begin{bmatrix} \sin(\gamma_{r,k})e^{j\eta_{r,k}} \\ \cos(\gamma_{r,k}) \end{bmatrix} \tag{4b}$$

where $\gamma_{t,k}, \gamma_{r,k} \in [0\ \pi/2)$ are the polarization angles, $\eta_{t,k}, \eta_{r,k} \in [-\pi\ \pi)$ are the polarization phase difference. Besides,

$$\left\|\mathbf{c}_{t_1,k}\right\|_{\mathrm{F}} = \left\|\mathbf{c}_{t_2,k}\right\|_{\mathrm{F}} = \left\|\mathbf{c}_{r_1,k}\right\|_{\mathrm{F}} = \left\|\mathbf{c}_{r_2,k}\right\|_{\mathrm{F}} = 1 \tag{5}$$

and

$$\mathbf{v}_t = \frac{\mathbf{c}_{t_1,k}}{\left\|\mathbf{c}_{t_1,k}\right\|_F} \circledast \frac{\mathbf{c}^*_{t_2,k}}{\left\|\mathbf{c}_{t_2,k}\right\|_F} = \begin{bmatrix} \sin(\theta_{t,k})\cos(\phi_{t,k}) \\ \sin(\theta_{t,k})\sin(\phi_{t,k}) \\ \cos(\theta_{t,k}) \end{bmatrix} \tag{6a}$$

$$\mathbf{v}_r = \frac{\mathbf{c}_{r_1,k}}{\left\|\mathbf{c}_{r_1,k}\right\|_F} \circledast \frac{\mathbf{c}^*_{r_2,k}}{\left\|\mathbf{c}_{r_2,k}\right\|_F} = \begin{bmatrix} \sin(\theta_{r,k})\cos(\phi_{r,k}) \\ \sin(\theta_{r,k})\sin(\phi_{r,k}) \\ \cos(\theta_{r,k}) \end{bmatrix} \tag{6b}$$

Then the received signal in the lth snapshot can be expressed as [17]

$$\mathbf{X}_l = \mathbf{B}_r \mathbf{\Lambda}_l \mathbf{B}_t^{\mathrm{T}} \mathbf{S} + \mathbf{N}_l \tag{7}$$

where $\mathbf{B}_r = [\mathbf{b}_{r,1}, \mathbf{b}_{r,2}, \cdots, \mathbf{b}_{r,K}] = \mathbf{A}_r \odot \mathbf{C}_r \in \mathbb{C}^{6N\times K}$, $\mathbf{B}_t = [\mathbf{b}_{t,1}, \mathbf{b}_{t,2}, \cdots, \mathbf{b}_{t,K}] = \mathbf{A}_t \odot \mathbf{C}_t \in \mathbb{C}^{6M\times K}$ are the transmit and receive array manifold, respectively, in which $\mathbf{A}_r = [\mathbf{a}_{r,1}, \mathbf{a}_{r,2}, \cdots, \mathbf{a}_{r,K}] \in \mathbb{C}^{N\times K}$, $\mathbf{C}_r = [\mathbf{c}_{r,1}, \mathbf{c}_{r,2}, \cdots, \mathbf{c}_{r,K}] \in$

$\mathbb{C}^{6\times K}$, $\mathbf{A}_t = [\mathbf{a}_{t,1}, \mathbf{a}_{t,2}, \cdots, \mathbf{a}_{t,K}] \in \mathbb{C}^{M\times K}$, and $\mathbf{C}_t = [\mathbf{c}_{t,1}, \mathbf{c}_{t,2}, \cdots, \mathbf{c}_{t,K}] \in \mathbb{C}^{6\times K}$; $\mathbf{\Lambda}_l = \mathrm{diag}(\mathbf{s}_l^{'})$, in which $\mathbf{s}_l^{'} = [\rho_1(l), \rho_2(l), \cdots, \rho_K(l)] \in \mathbb{C}^{K\times 1}$ and $\rho_k(l)$ stands for the reflection coefficient of the kth target during the lth snapshot, $\mathbf{S} \in \mathbb{C}^{6M\times Q}$ are the orthogonal signal emitted by the transmit arrays, and $\mathbf{N}_l \in \mathbb{C}^{6N\times Q}$ stands for the noise matrix. The output of matched filters can be expressed as

$$\mathbf{Y}_l = \mathbf{X}_l\mathbf{S}^{\mathrm{H}}\left[\mathbf{S}\mathbf{S}^{\mathrm{H}}\right]^{-1} = \mathbf{B}_r\mathbf{\Lambda}_l\mathbf{B}_t^{\mathrm{T}} + \mathbf{N}_l^{'} \tag{8}$$

where $\mathbf{N}_l^{'} = \mathbf{N}_l\mathbf{S}^{\mathrm{H}}(\mathbf{S}\mathbf{S}^{\mathrm{H}})^{-1}$ is the noise matrix after matched filters.

3. Signal subspace acquisition method

3.1. Definitions related to tensor

First, some definition and properties about tensor are introduced for the following analysis, which is present in [22].

Definition 1. (Unfolding or Matrixcization)

The mode-n unfolding of an N-th order tensor $\mathcal{X} \in \mathbb{C}^{I_1\times I_2\times\cdots\times I_N}$ is denoted by $\mathcal{X}_{(n)}$. The $(i_1, i_2, \cdots, i_N)$ element of $\mathcal{X}$ maps to the (i_n, j)th element of $\mathcal{X}_{(n)}$, where

$$j = 1 + \sum_{k=1,k\neq n}^{N}\left[(i_k - 1)\left(\prod_{m=1,m\neq n}^{k-1} I_m\right)\right] \tag{9}$$

Definition 2. (Mode-n tensor-matrix product)

The mode-n product of an N-th order $\mathcal{X} \in \mathbb{C}^{I_1\times I_2\times\cdots\times I_N}$ with a matrix $\mathbf{A} \in \mathbb{C}^{J_n\times I_n}$ is denoted by $\mathcal{Y} = \mathcal{X}\times_n\mathbf{A}$, where $\mathcal{Y} \in \mathbb{C}^{I_1\times I_2\times\cdots\times I_{n-1}\times J_n\times I_{n+1}\times\cdots\times I_N}$ and $\mathcal{Y}_{i_1,i_2,\cdots,i_{n-1},j_n,\cdots,i_N} = \sum_{i_n=1}^{I_n}\mathcal{X}_{i_1,i_2,\cdots,i_{n-1},i_n,\cdots,i_N}a_{j_n,i_n}$. Moreover, the mode-n product satisfies the following properties

$$\mathcal{X}\times_m\mathbf{A}\times_n\mathbf{B} = \mathcal{X}\times_n\mathbf{B}\times_m\mathbf{A}, (m\neq n) \tag{10}$$

$$\mathcal{X}\times_n\mathbf{A}\times_n\mathbf{B} = \mathcal{X}\times_n(\mathbf{B}\mathbf{A}), \mathbf{A} \in C^{J\times I_n}, \mathbf{B} \in \mathbb{C}^{I_n\times J} \tag{11}$$

$$\begin{aligned}&[\mathcal{X}\times_1\mathbf{A}_1\times_2\mathbf{A}_2\times\cdots\times_N\mathbf{A}_N]_{(n)} = \\ &\mathbf{A}_n\cdot\mathcal{X}_{(n)}\cdot[\mathbf{A}_{n+1}\otimes\mathbf{A}_{n+2}\cdots\otimes\mathbf{A}_N\otimes\mathbf{A}_1\cdots\otimes\mathbf{A}_{n-1}]^{\mathrm{T}}\end{aligned} \tag{12}$$

Definition 3. (High-order SVD, HOSVD)

The HOSVD of an N-th order tensor $\mathcal{X} \in \mathbb{C}^{I_1 \times I_2 \times \cdots I_N}$ is given by $\mathcal{X} = \mathcal{G} \times_1 \mathbf{U}_1 \times_2 \mathbf{U}_2 \times_3 \cdots \times_N \mathbf{U}_N$, where $\mathbf{U}_n \in \mathbb{C}^{I_n \times I_n}$ represents the left singular matric obtained by performing SVD on $\mathcal{X}_{(n)}$, i.e, $\{\mathcal{X}_{(n)} = \mathbf{U}_n \mathbf{\Sigma}_n \mathbf{V}_n^{\mathrm{H}}\}_{n=1}^{N}$, $\mathcal{G} \in \mathbb{C}^{I_1 \times I_2 \times \cdots \times I_N}$ is the core tensor which satisfies the all orthogonality conditions. Meanwhile, the core tensor can be written as $\mathcal{G} = \mathcal{X} \times_1 \mathbf{U}_1^{\mathrm{H}} \times_2 \mathbf{U}_2^{\mathrm{H}} \times_3 \cdots \times_N \mathbf{U}_N^{\mathrm{H}}$.

3.2. proposed signal subspace acquisition method

Generally, the signal subspace can be obtained by the following ways: (1)Perform SVD on the data matrix or EVD on the covariance matrix of the data matrix to get the signal subspace; (2)Adopt the propagation method to get the signal subspace through the covariance matrix of the data matrix; (3) Perform HOSVD on the data tensor or the covariance tensor of the data tensor to get the signal subspace. The signal subspace mentioned above generally refers to that spans the same space as the receive-transmit array manifold.

When $36NM > L$, we directly perform SVD or HOSVD on the data matrix or data tensor to save computation load [7]. Otherwise, we perform EVD or HOSVD on the covariance matrix of the data matrix or the covariance tensor of the data tensor. The process that through performing EVD on covariance matrix, performing HOSVD on covariance tensor and PM to get the signal subspace have been introduced in the literatures [17, 18, 19], respectively. This paper only presents the approach that performs SVD or HOSVD on the data matrix or the data tensor to get the signal subspace.

First, we introduce the method that directly performs SVD on the data matrix. In order to take advantage of the high degree of freedom of the MIMO radar, the received data matrix in each snapshot (8) is straightened into a column vector, and then (8) can be rewritten as

$$\mathbf{y}_l = \mathrm{vec}(\mathbf{Y}_l) = [\mathbf{B}_r \odot \mathbf{B}_t]\mathbf{s}_l^{'} + \mathbf{n}^{'}(l) = \mathbf{B}_{rt}\mathbf{s}_l^{'} + \mathbf{n}_l^{'} \tag{13}$$

where $\mathbf{B}_{rt} = [\mathbf{B}_r \odot \mathbf{B}_t] \in \mathbb{C}^{36MN \times K}$ is the joint receive-transmit array manifold and $\mathbf{n}_l^{'} = \mathrm{vec}(\mathbf{N}_l^{'}) \in \mathbb{C}^{36MN \times 1}$. Suppose the number of snapshots is L, then the received multi-snapshot data can be written into the matrix form as

$$\mathbf{Y} = [\mathbf{y}_1, \mathbf{y}_2, \cdots, \mathbf{y}_L] \in \mathbb{C}^{36MN \times L} = \mathbf{B}_{rt}\mathbf{S}^{'} + \mathbf{N}^{'} \tag{14}$$

where $\mathbf{S}^{'} = [\mathbf{s}_1^{'}, \mathbf{s}_2^{'}, \cdots, \mathbf{s}_L^{'}] \in \mathbb{C}^{K \times L}$ and $\mathbf{N}^{'} = [\mathbf{n}_l^{'}, \mathbf{n}_2^{'}, \cdots, \mathbf{n}_L^{'}] \in \mathbb{C}^{36MN \times L}$. The SVD of $\mathbf{Y}$ can be expressed as $\mathbf{Y} = \mathbf{U}\mathbf{\Lambda}\mathbf{V}$, the left singular value vectors corresponding to the firstK large singular values are selected to form

the signal subspace (marked as $\mathbf{U}_{ys}$). It is clear that $\mathbf{U}_{ys}$ spans the same space as the joint receive-transmit array manifold $\mathbf{B}_{rt}$.

Next, we introduce the method that directly performs HOSVD on the received data tensor. By stacking the matrices $\mathbf{Y}_l, (l = 1, 2, \cdots, L)$ along the third dimension to construct a data tensor $\mathcal{Y} \in \mathbb{C}^{6N \times 6M \times L}$, which is given by

$$\mathcal{Y}_{::l} = \mathbf{B}_r \mathbf{\Lambda}_l \mathbf{B}_t^{\mathrm{T}} + \mathbf{N}_l^{'} \tag{15}$$

And we have $\mathbf{Y} = \left[\mathcal{Y}_{(3)}\right]^{\mathrm{T}}$ [7]. As introduced in [7], the signal subspace is estimated by direct processing on the measurement tensor $\mathcal{Y}$ when $36MN > L$. The HOSVD of $\mathcal{Y}$ can be expressed as

$$\mathcal{Y} = \mathcal{G} \times_1 \mathbf{U}_1 \times_2 \mathbf{U}_2 \times_3 \mathbf{U}_3 \tag{16}$$

where $\mathcal{G} \in C^{6N \times 6M \times L}$ stands for the core tensor and $\mathbf{U}_i, (i = 1, 2, 3)$ is the left singular vector matrix of the i-mode matrix unfolding of $\mathcal{Y}$ as $\{\mathcal{Y}_{(i)} = \mathbf{U}_i \Sigma_i \mathbf{V}_i^{\mathrm{H}}\}_{i=1}^{3}$. Then we can define a subspace tensor $\mathcal{U}$ as

$$\mathcal{U} = \mathcal{G}_s \times_1 \mathbf{U}_{1s} \times_2 \mathbf{U}_{2s} \tag{17}$$

where $\mathcal{G}_s = \mathcal{Y} \times_1 \mathbf{U}_{1s}^{\mathrm{H}} \times_2 \mathbf{U}_{2s}^{\mathrm{H}} \times_3 \mathbf{U}_{3s}^{\mathrm{H}} \in \mathbb{C}^{K \times K \times K}$ represents the signal component in $\mathcal{G}$, and the column vectors in $\mathbf{U}_{is}, (i = 1, 2)$ are composed of the singular vectors in $\mathbf{U}_i, (i = 1, 2)$ corresponding to the first K large singular values. Insert $\mathcal{G}_s$ into eq(17), and combine with the definition 1, we have

$$\mathcal{U} = \mathcal{Y} \times_1 \left(\mathbf{U}_{1s}\mathbf{U}_{1s}^{\mathrm{H}}\right) \times_2 \left(\mathbf{U}_{2s}\mathbf{U}_{2s}^{\mathrm{H}}\right) \times_3 \mathbf{U}_{3s}^{\mathrm{H}} \tag{18}$$

Then the signal subspace is given by $\mathbf{U}_{hs} = [\mathcal{U}_{(3)}]^{\mathrm{T}}$, by utilizing eq(18) and definition 1, we have

$$\mathbf{U}_{hs} = \left[(\mathbf{U}_{1s}\mathbf{U}_{1s}^{\mathrm{H}}) \otimes (\mathbf{U}_{2s}\mathbf{U}_{2s}^{\mathrm{H}})\right] \mathbf{Y}\mathbf{U}_{3s}^{*} \tag{19}$$

Where $\mathbf{Y} = \left[\mathcal{Y}_{(3)}\right]^{\mathrm{T}}$. Genearlly, the signal subspace can be estimated by using the truncated SVD of $\mathbf{Y}$, i.e. $\mathbf{Y} \approx \mathbf{U}_{ys}\mathbf{\Sigma}_{ys}\mathbf{V}_{ys}^{H}$, insert it into eq(19), we have

$$\mathbf{U}_{hs} = \left[(\mathbf{U}_{1s}\mathbf{U}_{1s}^{\mathrm{H}}) \otimes (\mathbf{U}_{2s}\mathbf{U}_{2s}^{\mathrm{H}})\right] \mathbf{U}_{ys}\mathbf{\Sigma}_{ys}\mathbf{V}_{ys}^{\mathrm{H}}\mathbf{U}_{3s}^{*} \tag{20}$$

Due to $\mathcal{Y}_{(3)} = \mathbf{U}_{3s}\mathbf{\Sigma}_{3s}\mathbf{V}_{3s}^{\mathrm{H}}$ and $\mathbf{Y} = \left[\mathcal{Y}_{(3)}\right]^{\mathrm{T}}$, we have $\mathbf{U}_{3s}^{*} = \mathbf{V}_{ys}$ and $\mathbf{\Sigma}_{ys} = \mathbf{\Sigma}_{3s}$. To simplify analysis, we multiply eq(19) by $\mathbf{\Sigma}_{3s}^{-1}$. Therefore, eq(20) can be rewritten as

$$\mathbf{U}_{hs} = \left[(\mathbf{U}_{1s}\mathbf{U}_{1s}^{\mathrm{H}}) \otimes (\mathbf{U}_{2s}\mathbf{U}_{2s}^{\mathrm{H}})\right] \mathbf{U}_{ys} \tag{21}$$

Eq(21) describes the relationship between $\mathbf{U}_{hs}$ and $\mathbf{U}_{ys}$, where $\mathbf{U}_{hs}$ is the projection of $\mathbf{U}_{ys}$ on the Kronecker product of the space spanned by 1-mode vectors $\mathbf{U}_{1s}\mathbf{U}_{1s}^{\mathrm{H}}$ and space spanned by 2-mode vectors $\mathbf{U}_{2s}\mathbf{U}_{2s}^{\mathrm{H}}$. Like $\mathbf{U}_{ys}$, $\mathbf{U}_{hs}$ spans the same space as the joint receive-transmit array manifold $\mathbf{B}_{rt}$.

4. Parameter estimation approach

4.0.1. Previous signal subspace-based algorithms

As mentioned in the introduction, the ESPRIT algorithm in [17], the HOSVD algorithm in [18], and the PM algorithm in [19] are all selecting a part of the signal subspace to estimate all parameters. The signal subspace obtained by EVD in [17], HOSVD in [18], and PM in [19] are all marked as $\mathbf{U}_s$. When estimating the receive parameters, the selected part of the signal subspace can be expressed as

$$\mathbf{E}_r = \mathbf{J}_r\mathbf{U}_s \in \mathbb{C}^{6N\times K} \tag{22}$$

where $\mathbf{J}_r = [\mathbf{0}_{6N\times 6pN} \mid I_{6N} \mid \mathbf{0}_{6N\times(36NM-6(p+1)N)}]$ with $p = 0, 1, \cdots, 6M-1$. A diagonal matrix $\mathbf{\Phi}_r = \mathrm{diag}([e^{j\pi d_r \sin(\theta_{r,1})/\lambda}, e^{j\pi d_r \sin(\theta_{r,2})/\lambda}, \cdots, e^{j\pi d_r \sin(\theta_{r,K})/\lambda}])$ related to receive elevation angle is calculated using $\mathbf{E}_r$ by exploiting the rotation invariance of the receive array manifold. Then the receive spatial response vector $\mathbf{c}_{r,k}(k = 1, 2, \cdots, K)$ is recovered from $\mathbf{E}_r$ using the estimated diagonal matrix $\mathbf{\Phi}_r$. The receive elevation angle $\theta_{r,k}$ and azimuth angle $\phi_{r,k}$ are estimated using 'Vector Cross-Product' in [17, 18], receive polarization parameters γ_k and η_k are estimated via LS principle. Different from the receive elevation angle estimation in [17, 18], $\theta_{r,k}$ is calculated using the estimated diagonal matrix $\mathbf{\Phi}_r$. When estimating the transmit parameters, the selected part of the signal subspace can be expressed as

$$\mathbf{E}_t = \mathbf{J}_t\mathbf{U}_s \in \mathbb{C}^{6M\times K} \tag{23}$$

where $\mathbf{J}_t = [\mathbf{I}_{6M} \otimes \mathbf{e}_q^{\mathrm{T}}]$, in which $\mathbf{e}_q$ is a $6N \times 1$ vector with qth entry is one and others are zeros, and $q = 1, 2, \cdots, 6N$. Similarly, use $\mathbf{E}_t$ to calculate the diagonal matrix $\mathbf{\Phi}_t = \mathrm{diag}([e^{j\pi d_t \sin(\theta_{t,1})/\lambda}, e^{j\pi d_t \sin(\theta_{t,2})/\lambda}, \cdots, e^{j\pi d_t \sin(\theta_{t,K})/\lambda}])$ related to the transmit elevation angle by exploiting the rotation invariance of the transmit array manifold. The transmit spatial response vector $\mathbf{c}_{t,k}(k = 1, 2, \cdots, K)$ is recovered from $\mathbf{E}_t$ using the estimated diagonal matrix $\mathbf{\Phi}_t$. The transmit elevation angle $\theta_{t,k}$ and azimuth angle $\phi_{t,k}$ are estimated using 'Vector Cross-Product' in [17, 18], transmit polarization parameters γ_k and

η_k are estimated via LS principle. $\theta_{t,k}$ is also estimated using the estimated diagonal matrix $\mathbf{\Phi}_r$, and other parameters estimation is the same as that in [17, 18].

Different from the above three algorithms, the PM algorithm in [20] uses the 36NM rows of signal subspace to estimate the transmit and receive elevation angle by exploiting the rotation invariance of the joint receive-transmit array manifold, which will be introduced in the next section. But after that, the PM algorithm in [20] also just select a part of signal subspace as eq(22)/eq(23) to estimate the receive/transmit azimuth angle and polarization parameters by adopting the 'Vector Cross-Product' and LS ideas in [17].

It can be seen from the above analysis that all methods based on signal subspace only select 6N/6M rows of 36NM rows in the signal subspace to estimate all transmit/receive parameters, except for the PM algorithm in [20] use the whole signal subspace to estimate the transmit and receive elevation angle. They only selected a small part of the signal subspace and wast most of the signal subspace. Besides, as shown in [17], the accuracy of the transmit and receive parameter estimation is also related to the value of p and q, and different values of p and q will bring different estimation results.

4.0.2. Proposed signal subspace-based approach

To make full use of the entire signal subspace, we propose an improved approach applicable to all signal subspace-based algorithms where the all parameters are estimated by usig the 36NM rows of the signal subspace, instead of 6N/6M rows of the signal subspace.

No matter which method is used to obtain the signal subspace, all of them are uniformly denoted as $\hat{\mathbf{U}}_s$ for the convenience of the following expressions. From the analysis in [20], we know that $\hat{\mathbf{U}}_s$ spans the same space as $\mathbf{B}_{rt}$. Therefore, there excite a full-rank matrix satisfying

$$\mathbf{B}_{r,t} = \hat{\mathbf{U}}_s \mathbf{\Gamma} \tag{24}$$

Define four selection matrices as

$$\begin{cases} \mathbf{J}_1 = [\mathbf{I}_{N-1} \ \mathbf{0}_{(N-1)\times 1}] \otimes \mathbf{I}_{36M} \\ \mathbf{J}_2 = [\mathbf{0}_{(N-1)\times 1} \ \mathbf{I}_{N-1}] \otimes \mathbf{I}_{36M} \end{cases} \tag{25a}$$

$$\begin{cases} \mathbf{J}_3 = \mathbf{I}_{36N} \otimes [\mathbf{I}_{M-1} \ \mathbf{0}_{(M-1)\times 1}] \\ \mathbf{J}_4 = \mathbf{I}_{36N} \otimes [\mathbf{0}_{(M-1)\times 1} \ \mathbf{I}_{M-1}] \end{cases} \tag{25b}$$

Then we can find that

$$\mathbf{J}_2\mathbf{B}_{r,t} = \mathbf{J}_1\mathbf{B}_{r,t}\mathbf{\Phi}_r \tag{26a}$$

$$\mathbf{J}_4\mathbf{B}_{r,t} = \mathbf{J}_3\mathbf{B}_{r,t}\mathbf{\Phi}_t \tag{26b}$$

where $\mathbf{\Phi}_r$ and $\mathbf{\Phi}_t$ have been given above. Insert (24) into (26), we have

$$\mathbf{J}_2\hat{\mathbf{U}}_s\mathbf{\Gamma} = \mathbf{J}_1\hat{\mathbf{U}}_s\mathbf{\Gamma}\mathbf{\Phi}_r \tag{27a}$$

$$\mathbf{J}_4\hat{\mathbf{U}}_s\mathbf{\Gamma} = \mathbf{J}_3\hat{\mathbf{U}}_s\mathbf{\Gamma}\mathbf{\Phi}_t \tag{27b}$$

Then, we calculate

$$\mathbf{\Psi}_r = (\mathbf{J}_1\hat{\mathbf{U}}_s)^\dagger\mathbf{J}_2\hat{\mathbf{U}}_s = \mathbf{\Gamma}\mathbf{\Phi}_r\mathbf{\Gamma}^{-1} \tag{28a}$$

$$\mathbf{\Psi}_t = (\mathbf{J}_3\hat{\mathbf{U}}_s)^\dagger\mathbf{J}_4\hat{\mathbf{U}}_s = \mathbf{\Gamma}\mathbf{\Phi}_t\mathbf{\Gamma}^{-1} \tag{28b}$$

Perform eigenvalue decomposition on $\mathbf{\Psi}_r$ and $\mathbf{\Psi}_t$, respectively. Mark their eigenvalues as $\hat{\mathbf{\Phi}}_r$ and $\hat{\mathbf{\Phi}}_t$, respectively, and mark the corresponding eigenvectors as $\hat{\mathbf{\Gamma}}_1$ and $\hat{\mathbf{\Gamma}}_2$. It is easy to see that $\hat{\mathbf{\Phi}}_r$, $\hat{\mathbf{\Phi}}_t$, $\hat{\mathbf{\Gamma}}_1$ and $\hat{\mathbf{\Gamma}}_2$ are the estimates of $\mathbf{\Phi}_r$, $\mathbf{\Phi}_t$, $\mathbf{\Gamma}$, respectively. Due to the non-uniqueness of eigenvalue decomposition, the position of diagonal elements of $\hat{\mathbf{\Phi}}_r$ and $\mathbf{\Phi}_r$ may be different, so do $\hat{\mathbf{\Phi}}_t$ and $\mathbf{\Phi}_t$ are. To ensure the paired estimation of the transmit and the receive elevation angle, we adopt the joint diagonalization of $\mathbf{\Psi}_r$ and $\mathbf{\Psi}_t$. A common approach is to perform EVD on one of the matrices and use its eigenvectors matrix to diagonalize the other matrix, i.e.

$$\mathbf{\Psi}_r = \hat{\mathbf{\Gamma}}\hat{\mathbf{\Phi}}_r\hat{\mathbf{\Gamma}}^{-1} \tag{29a}$$

$$\hat{\mathbf{\Phi}}_r = \hat{\mathbf{\Gamma}}^{-1}\mathbf{\Psi}_r\hat{\mathbf{\Gamma}} \tag{29b}$$

where $\hat{\mathbf{\Phi}}_r = \mathrm{diag}(\hat{\lambda}_{r,1}, \hat{\lambda}_{r,2}, \cdots, \hat{\lambda}_{r,K})$ and $\hat{\mathbf{\Phi}}_t = \mathrm{diag}(\hat{\lambda}_{t,1}, \hat{\lambda}_{t,2}, \cdots, \hat{\lambda}_{t,K})$. The transmit and receive elevation angles can be obtained via

$$\hat{\theta}_{r,k} = \arcsin\{\mathrm{angle}(\hat{\lambda}_{r,k})\lambda/(2d_r)\} \tag{30a}$$

$$\hat{\theta}_{t,k} = \arcsin\{\mathrm{angle}(\hat{\lambda}_{t,k})\lambda/(2d_t)\} \tag{30b}$$

The elevation angle estimation process introduced above is all almost the same as that in [20], except the joint diagonalization process. After obtaining elevation angle estimates, we start to recover the spatial response vectors $\mathbf{c}_{r,k}$ and $\mathbf{c}_{t,k}$ from the 36NM rows of the signal subspace to estimate

other parameters, instead of from the 6N or 6M rows of the signal subspace. This approach is entirely different from all previous methods based on signal subspace.

The joint receive-transmit array manifold can be recovered via

$$\hat{\mathbf{B}}_{rt} = \mathbf{U}_s \hat{\mathbf{\Gamma}} \tag{31}$$

In fact, by using the property of Kronecker-product, the joint receive-transmit steering vector can be rewritten as

$$\begin{aligned} \mathbf{a}_{rt,k} &= (\mathbf{a}_{r,k} \otimes \mathbf{c}_{r,k}) \otimes (\mathbf{a}_{t,k} \otimes \mathbf{c}_{t,k}) \\ &= [(\mathbf{a}_{r,k} \otimes \mathbf{I}_6)\, \mathbf{c}_{r,k}] \otimes [(\mathbf{a}_{t,k} \otimes \mathbf{I}_6)\, \mathbf{c}_{t,k}] \\ &= [(\mathbf{a}_{r,k} \otimes \mathbf{I}_6) \otimes (\mathbf{a}_{t,k} \otimes \mathbf{I}_6)]\, (\mathbf{c}_{r,k} \otimes \mathbf{c}_{t,k}) \end{aligned} \tag{32}$$

Let $\mathbf{c}_{rt,k} = \mathbf{c}_{r,k} \otimes \mathbf{c}_{t,k}$ denotes the joint receive-transmit spatial response vector of the kth target. Since the elevation angle estimation $(\hat{\theta}_{r,k}, \hat{\theta}_{t,k})$ and the joint receive-transmit array manifold estimation use the same matrix $\hat{\mathbf{\Gamma}}$, thus the elevation angle estimation of the kth target and the joint receive-transmit array vector $\hat{\mathbf{B}}_{rt}(:,k)$ are paired, in which $\hat{\mathbf{B}}_{rt}(:,k)$ is the kth column of matrix $\hat{\mathbf{B}}_{rt}$. By utilizing (32), $\mathbf{c}_{rt,k}$ can be estimated by last-squares (LS) principle via

$$\min_{\mathbf{c}_{rt,k}} \left\| [(\hat{\mathbf{a}}_{r,k} \otimes \mathbf{I}_6) \otimes (\hat{\mathbf{a}}_{t,k} \otimes \mathbf{I}_6)]\, \mathbf{c}_{rt,k} - \hat{\mathbf{B}}_{rt}(:,k) \right\|_{\mathrm{F}}^2 \tag{33}$$

where $\hat{\mathbf{a}}_{r,k} = [1,\, \hat{\lambda}_{r,k}, \cdots, \hat{\lambda}_{r,k}^{N-1}]^{\mathrm{T}}$ and $\hat{\mathbf{a}}_{t,k} = [1,\, \hat{\lambda}_{t,k}, \cdots, \hat{\lambda}_{t,k}^{M-1}]^{\mathrm{T}}$. The LS solution for $\mathbf{c}_{rt,k}$ is

$$\hat{\mathbf{c}}_{rt,k} = ([(\hat{\mathbf{a}}_{r,k} \otimes \mathbf{I}_6) \otimes (\hat{\mathbf{a}}_{t,k} \otimes \mathbf{I}_6)])^{\dagger}\, \hat{\mathbf{B}}_{rt}(:,k) \tag{34}$$

Combine $\mathbf{c}_{rt,k} = \mathbf{c}_{r,k} \otimes \mathbf{c}_{t,k}$, so $\hat{\mathbf{c}}_{rt,k}$ can be rewritten as $\hat{\mathbf{c}}_{rt,k} = \hat{\mathbf{c}}_{r,k} \otimes \hat{\mathbf{c}}_{t,k}$, in which $\hat{\mathbf{c}}_{r,k} \in \mathbb{C}^{6\times 1}$ and $\hat{\mathbf{c}}_{t,k} \in \mathbb{C}^{6\times 1}$ are the estimates of $\mathbf{c}_{r,k}$ and $\mathbf{c}_{t,k}$, respectively. Let $\mathbf{c}_{r,k}^{'}$ and $\mathbf{c}_{t,k}^{'}$ be the rough estimates of $\hat{\mathbf{c}}_{r,k}$ and $\hat{\mathbf{c}}_{t,k}$, respectively, and they can be calculated via

$$\begin{aligned} \hat{\mathbf{c}}_{r,k}^{'}(j,1) =& \frac{1}{6} \sum_{j=1}^{6} \hat{\mathbf{c}}_{rt,k}(6j-5:6j,1)(j=1,2,\cdots,6) \\ =& \frac{1}{6} \sum_{j=1}^{6} \hat{\mathbf{c}}_{t,k}(j,1)\hat{\mathbf{c}}_{r,k} = \hat{c}_{t,k}^{s}\hat{\mathbf{c}}_{r,k} \end{aligned} \tag{35a}$$

$$\begin{aligned}\hat{\mathbf{c}}_{t,k}^{'}(j,1) =&\frac{1}{6}\sum_{i=1}^{6}\hat{\mathbf{c}}_{rt,k}(6(i-1)+j,1)(j=1,2,\cdots,6)\\ =&\frac{1}{6}\sum_{i=1}^{6}\hat{\mathbf{c}}_{r,k}(j,1)\hat{\mathbf{c}}_{t,k}=\hat{c}_{r,k}^{s}\hat{\mathbf{c}}_{t,k}\end{aligned} \tag{35b}$$

where $\hat{c}_{t,k}^{s}=\frac{1}{6}\sum_{j=1}^{6}\hat{\mathbf{c}}_{t,k}(j,1)$ and $\hat{c}_{r,k}^{s}=\frac{1}{6}\sum_{j=1}^{6}\hat{\mathbf{c}}_{r,k}(j,1)$. It should be emphasized that $\hat{\mathbf{c}}_{r,k}^{'}$ is the product of the vector $\hat{\mathbf{c}}_{r,k}$ and the complex number $\hat{c}_{t,k}^{s}$, and $\hat{\mathbf{c}}_{t,k}^{'}$ is the product of the vector $\hat{\mathbf{c}}_{t,k}$ and the complex number $\hat{c}_{r,k}^{s}$. After obtaining the estimated $\hat{\mathbf{c}}_{r,k}$ and $\hat{\mathbf{c}}_{t,k}$, the azimuth angle and the polariztion parameters can be estimated through 'Vector Cross-Product' method in [17]. Let $\hat{\mathbf{c}}_{r_1,k}^{'}\in\mathbb{C}^{3\times1}$ and $\hat{\mathbf{c}}_{r_2,k}^{'}\in\mathbb{C}^{3\times1}$ be the first and last three elements of $\hat{\mathbf{c}}_{r,k}^{'}$, respectively. And let $\hat{\mathbf{c}}_{t_1,k}^{'}\in\mathbb{C}^{3\times1}$ and $\hat{\mathbf{c}}_{t_2,k}^{'}\in\mathbb{C}^{3\times1}$ be the first and last three elements of $\hat{\mathbf{c}}_{t,k}^{'}$, respectively. Utilize (6), we can estimate $\mathbf{v}_{r,k}$ and $\mathbf{v}_{t,k}$ via

$$\begin{aligned}\hat{\mathbf{v}}_{r,k} =&\frac{\hat{\mathbf{c}}_{r_1,k}^{'}}{\left\|\hat{\mathbf{c}}_{r_1,k}^{'}\right\|_{\mathrm{F}}}\circledast\frac{\hat{\mathbf{c}}_{r_2,k}^{'*}}{\left\|\hat{\mathbf{c}}_{r_2,k}^{'}\right\|_{\mathrm{F}}}=\frac{\hat{c}_{t,k}^{s}\hat{\mathbf{c}}_{r_1,k}}{\left\|\hat{c}_{t,k}^{s}\hat{\mathbf{c}}_{r_1,k}\right\|_{\mathrm{F}}}\circledast\frac{\hat{c}_{t,k}^{s*}\hat{\mathbf{c}}_{r_2,k}^{*}}{\left\|\hat{c}_{t,k}^{s}\hat{\mathbf{c}}_{r_2,k}\right\|_{\mathrm{F}}}\\ =&\frac{\hat{\mathbf{c}}_{r_1,k}}{\left\|\hat{\mathbf{c}}_{r_1,k}\right\|_{\mathrm{F}}}\circledast\frac{\hat{\mathbf{c}}_{r_2,k}^{*}}{\left\|\hat{\mathbf{c}}_{r_2,k}\right\|_{\mathrm{F}}}=\begin{bmatrix}\sin(\hat{\theta}_{r,k})\cos(\hat{\phi}_{r,k})\\ \sin(\hat{\theta}_{r,k})\sin(\hat{\phi}_{r,k})\\ \cos(\hat{\theta}_{r,k})\end{bmatrix}\end{aligned} \tag{36a}$$

$$\begin{aligned}\hat{\mathbf{v}}_{t,k} =&\frac{\hat{\mathbf{c}}_{t_1,k}^{'}}{\left\|\hat{\mathbf{c}}_{t_1,k}^{'}\right\|_{\mathrm{F}}}\circledast\frac{\hat{\mathbf{c}}_{t_2,k}^{'*}}{\left\|\hat{\mathbf{c}}_{t_2,k}^{'}\right\|_{\mathrm{F}}}=\frac{\hat{c}_{r,k}^{s}\hat{\mathbf{c}}_{t_1,k}}{\left\|\hat{c}_{r,k}^{s}\hat{\mathbf{c}}_{t_1,k}\right\|_{\mathrm{F}}}\circledast\frac{\hat{c}_{r,k}^{s*}\hat{\mathbf{c}}_{t_2,k}^{*}}{\left\|\hat{c}_{r,k}^{s}\hat{\mathbf{c}}_{t_2,k}\right\|_{\mathrm{F}}}\\ =&\frac{\hat{\mathbf{c}}_{t_1,k}}{\left\|\hat{\mathbf{c}}_{t_1,k}\right\|_{\mathrm{F}}}\circledast\frac{\hat{\mathbf{c}}_{t_2,k}^{*}}{\left\|\hat{\mathbf{c}}_{t_2,k}\right\|_{\mathrm{F}}}=\begin{bmatrix}\sin(\hat{\theta}_{t,k})\cos(\hat{\phi}_{t,k})\\ \sin(\hat{\theta}_{t,k})\sin(\hat{\phi}_{t,k})\\ \cos(\hat{\theta}_{t,k})\end{bmatrix}\end{aligned} \tag{36b}$$

where $\hat{\mathbf{c}}_{r_1,k}$ and $\hat{\mathbf{c}}_{r_2,k}$ are the first and last three elements of $\hat{\mathbf{c}}_{r,k}$, respectively. $\hat{\mathbf{c}}_{t_1,k}$ and $\hat{\mathbf{c}}_{t_2,k}$ are the first and last three elements of $\hat{\mathbf{c}}_{t,k}$, respectively. As we can see from Eq.(36), $\hat{c}_{t,k}^{s}$ in $\hat{\mathbf{c}}_{r,k}^{'}$ and $\hat{c}_{r,k}^{s}$ in $\hat{\mathbf{c}}_{t,k}^{'}$ can be eliminated by 'Vector Cross-Product'. The following receive/transmit azimuth angle estimation will not be affected by $\hat{c}_{t,k}^{s}/\hat{c}_{r,k}^{s}$.

Then, $\phi_{r,k}$ and $\phi_{t,k}$ can be estimated by

$$\hat{\phi}_{r,k}=\arctan\left(\frac{\hat{\mathbf{v}}_{r,k}(2)}{\hat{\mathbf{v}}_{r,k}(1)}\right) \tag{37a}$$

$$\hat{\phi}_{t,k} = \arctan\left(\frac{\hat{\mathbf{v}}_{t,k}(2)}{\hat{\mathbf{v}}_{t,k}(1)}\right) \tag{37b}$$

Once $(\hat{\theta}_{r,k}, \hat{\phi}_{r,k})$ and $(\hat{\theta}_{t,k}, \hat{\phi}_{t,k})$ are obtained, we can construct the transmit and receive spatial angular matrices $\hat{\mathbf{F}}_{r,k}$ and $\hat{\mathbf{F}}_{t,k}$ according to (3), respectively. Then, $\mathbf{h}_{r,k}$ and $\mathbf{h}_{t,k}$ can be estimated via

$$\hat{\mathbf{h}}_{r,k} = \hat{\mathbf{F}}_{r,k}^{\dagger}\hat{\mathbf{c}}_{r,k}^{'} = \hat{c}_{t,k}^{s}\begin{bmatrix}\sin\left(\hat{\gamma}_{r,k}\right)e^{j\hat{\eta}_{r,k}} \\ \cos\left(\hat{\gamma}_{r,k}\right)\end{bmatrix} \tag{38a}$$

$$\hat{\mathbf{h}}_{t,k} = \hat{\mathbf{F}}_{t,k}^{\dagger}\hat{\mathbf{c}}_{t,k}^{'} = \hat{c}_{r,k}^{s}\begin{bmatrix}\sin\left(\hat{\gamma}_{t,k}\right)e^{j\hat{\eta}_{t,k}} \\ \cos\left(\hat{\gamma}_{t,k}\right)\end{bmatrix} \tag{38b}$$

Finally, $(\gamma_{r,k}, \eta_{r,k})$ and $(\gamma_{t,k}, \eta_{t,k})$ can be estimated via

$$\begin{cases}\hat{\gamma}_{r,k} = \arctan\left(\left|\dfrac{\hat{\mathbf{h}}_{r,k}(2)}{\hat{\mathbf{h}}_{r,k}(1)}\right|\right) \\ \hat{\eta}_{r,k} = \text{angle}\left(\dfrac{\hat{\mathbf{h}}_{r,k}(2)}{\hat{\mathbf{h}}_{r,k}(1)}\right)\end{cases} \tag{39a}$$

$$\begin{cases}\hat{\gamma}_{t,k} = \arctan\left(\left|\dfrac{\hat{\mathbf{h}}_{t,k}(2)}{\hat{\mathbf{h}}_{t,k}(1)}\right|\right) \\ \hat{\eta}_{t,k} = \text{angle}\left(\dfrac{\hat{\mathbf{h}}_{t,k}(2)}{\hat{\mathbf{h}}_{t,k}(1)}\right)\end{cases} \tag{39b}$$

From Eq.(39), we can know that when calculating $\hat{\gamma}_{r,k}$ and $\hat{\eta}_{r,k}$, $\hat{c}_{t,k}^{s}$ in $\hat{\mathbf{h}}_{r,k}$ can be eliminated by division, and the $\hat{c}_{r,k}^{s}$ in $\hat{\mathbf{h}}_{t,k}$ also can be eliminated by division when calculating $\hat{\gamma}_{t,k}$ and $\hat{\eta}_{t,k}$. The receive elevation angle estimate $\hat{\theta}_{t,k}(k = 1, 2, \cdots, K)$ and the transmit elevation angle estimate $\hat{\theta}_{t,k}$ are automatically paired by using joint diagonalization. Other receive and transmit parameters correspond one-to-one with the receive and transmit elevation angles, so the above algorithm can ensure automatic matching of all parameters. Although the azimuth angle and the polarization parameters are estimated by the 'Vector Cross-Product' and LS ideas like that in [17], respectively, we proved that the transmit/receive parameters does not affect the receive/transmit parameters estimation in the proposed approach, which is also not reflected in previous subspace-based algorithms.

5. Performance Analysis

5.1. Identifiability

When the proposed parameter estimation approach is applied to the signal subspace obtained by the two propsoed methods (marked the two algofithm as ImESPRIT-D algorithm and ImHOSVD-D algorithm, where the signal subsapce is obtained by performing SVD/HOSVD on data matrix/tensor), the elevation angles $\theta_{r,k}$ and $\theta_{t,k}$ are estimated by exploiting the invariant property of the virtual array manifold, and other receive/transmit parameters have a one-to-one correspondence with $\theta_{r,k}/\theta_{t,k}$. Thus, the maximum number of identifiable targets is limited by the rank of $\mathbf{\Psi}_r$ and $\mathbf{\Psi}_t$. When the signal subspace is obtained by directly performing SVD on the matrix $\mathbf{Y}$, the maximum rank of $\mathbf{\Psi}_r$ and $\mathbf{\Psi}_t$ are $36M(N-1)$ and $36N(M-1)$, respectively. Therefore, the maximum number of identifiable targets of the ESPRIT-data algorithm (marked as K_e) is

$$K_e = \min\{36M(N-1), 36N(M-1)\} \tag{40}$$

When the signal subspace is obtained by performing high-order SVD on the tensor $\mathcal{Y}$, the ranks of $\mathbf{\Psi}_r$ and $\mathbf{\Psi}_t$ are restricted by the ranks of $\mathbf{U}_{1s}$ and $\mathbf{U}_{2s}$, which is $\max\{6M, 6N\}$. Therefore, the maximum number of identifiable targets of the HOSVD-data algorithm (marked as K_h) is

$$K_h = \max\{6M, 6N\} \tag{41}$$

The identifiability of the ESPRIT alforithm in [17], the HOSVD algorithm in [18], and the PARAFAC algorithm in [21] are are $\min\{6(M-1), 6(N-1)\}$. The identifiability of the PM algorithm in [20] is $\min\{36M(N-1), 36N(M-1)\}$. Therefore, we can conclude that the identifiability of the proposed ESPRIT-data algorithm is the same as that of the PM algorithm, and both have better identifiability than other algorithms. Besides, the proposed HOSVD-data also has better identifiability than the ESPRIT, the HOSVD and the PARAFAC algorithms.

5.2. Computational Complexity

In the algorithm introduced in this article, the computation load is mainly concentrated in three processes, one is the signal subspace acquisition process, the second is the elevation angle estimation process, and the third is the spatial response vector recovery process. In the proposed signal subspace

Table 1: Computational complexity

Algorithm	Complexity
ImESPRIT-D	$\mathrm{O}\{108NMLK\} + 72K^2(2NM - M - N)$ $+37(36)^2NMK$
ImHOSVD-D	$\mathrm{O}\{324NMLK\} + 72K^2(2MN - N - M)$ $+37(36)^2NMK$
PARAFAC in [21]	$6n_pK^2(M + N + L) + 12K^2(N + M - 2)$ $+O\{K^3\}$
PM in [20]	$36^2N^2M^2L + 72K^2(3NM - N - M) + O\{K^3\}$
ESPRIT in [17]	$O\{36^3N^3M^3\} + 36^2N^2M^2K^2$
HOSVD in [18]	$O\{4 \times 36^3N^3M^3\} + 36^2N^2M^2K^2$

acquisition process, according to [7], the complexity of performing SVD on matrix $\mathbf{Y}$ is $O(36NMLK)$, the complexity of performing HOSVD on tensor $\mathcal{Y}$ is $O(3 \times 36NMLK)$. In the proposed parameter estimation process, the main complexity of elevation angle estimation process is $2\times36(N-1)MK^2+2K^3+2\times36(M-1)NK^2$. The main complexity of joint receive-transmit spatial response vector recovery process is $K[(36)^3NM + (36)^2NM]$. Let n_p be the number of iterations of the PARAFAC algorithm in [21]. Table 1 list the main computational loads of the proposed ImESPRIT-D algorithm, the proposed ImHOSVD-D algorithm, the PM in [20], the HOSVD algorithm in [18], and the ESPRIT algorithm in [17], the PARAFAC algorithm in [21]. It can be roughly judged from the table 1 that the computational complexity of directly performing SVD/HOSVD on the data matrix/tensor is lower than that of performing EVD/HOSVD on the covariance matrix/tensor. Therefore, the computational complexity of the proposed ImESPRIT-D and ImHOSVD-D is lower than that of ESPRIT and HOSVD, respectively.

5.3. Cramer-Rao bound (CRB)

Let $\Theta = [\theta_{r,1}, \cdots, \theta_{r,K}, \theta_{t,1}, \cdots, \eta_{t,K}] \in \mathbb{C}^{8K\times1}$ be the parameters needed to be estimated. According to [21], the CRB on Θ is given by

$$\mathrm{CRB} = \frac{\sigma^2}{2L}\left\{\mathrm{Re}\left[\left(\mathbf{B}_{rt,\Delta}^{\mathrm{H}}\mathbf{\Pi}_{\mathbf{B}_{rt}}^{\perp}\mathbf{B}_{rt,\Delta}\right)\oplus\left(\mathbf{R}_{\mathbf{S}'}^{\mathrm{T}}\otimes\mathbf{I}_8\right)\right]\right\}^{-1} \tag{42}$$

Where $\mathbf{\Pi}_{\mathbf{B}_{rt}}^{\perp} = \mathbf{I}_{36NM} - \mathbf{B}_{rt}(\mathbf{B}_{rt}^{\mathrm{H}}\mathbf{B}_{rt})^{-1}\mathbf{B}_{rt}^{\mathrm{H}}$, in which $\mathbf{B}_{rt}$ is the joint receive-transmit array manifold; $\mathbf{R}_{\mathbf{S}'} = \mathbf{S}'\mathbf{S}'^{\mathrm{H}}/L$, in which L is the number of pulses;

σ^2 is the noise power; $\mathbf{B}_{rt,\Delta} = \left[\frac{\partial \mathbf{B}_{rt}}{\partial \theta_{r,1}}, \cdots, \frac{\partial \mathbf{B}_{rt}}{\partial \theta_{r,K}}, \frac{\partial \mathbf{B}_{rt}}{\partial \theta_{t,1}}, \cdots, \frac{\partial \mathbf{B}_{rt}}{\partial \eta_{t,K}}\right]$. The detailed derivation process of CRB can be referred to [21].

6. Simulation

In this section, 200 Monte Carlo trials are taken to evaluate the performance of the proposed algorithm. The PM algorithm in [20], the ESPRIT algorithm in [17], the HOSVD algorithm in [18], the PARAFAC algorithm in [21] and the CRB are introduced as comparisons. Except for special instruction, the bistatic EMVS-MIMO radar is equipped with $M = 6$ transmit antennas and $N = 8$ receive antennas. Both the transmit and receive arrays are ULAs arranged in half-wavelength. The transmit baseband code matrix is $\mathbf{S} = (1 + j)/\sqrt{2}\mathbf{H}_{6M}$, where $\mathbf{H}_{6M}$ is composed of the first $6M$ rows of the $Q \times Q$ Hadamard matrix. Here, Q is set to 512. Suppose there are three uncorrelated far-field point-like targets. The angle information of these targets are $\boldsymbol{\theta}_t = (40°, 20°, 30°)$, $\boldsymbol{\phi}_t = (15°, 25°, 35°)$, $\boldsymbol{\gamma}_t = (10°, 22°, 35°)$, $\boldsymbol{\eta}_t = (36°, 48°, 56°)$, $\boldsymbol{\theta}_r = (24°, 38°, 16°)$, $\boldsymbol{\phi}_r = (21°, 32°, 55°)$, $\boldsymbol{\gamma}_r = (42°, 33°, 60°)$, $\boldsymbol{\eta}_r = (17°, 27°, 39°)$. The reflection coefficient of targets obey Gaussian distribution. The additive noise is assumed to be a spatial white complex Gaussian noise. The performance of the algorithm is evaluated by Root Mean Square Errors (RMSE), which is defined as

$$\text{RMSE} = \frac{1}{K}\sum_{k=1}^{K}\sqrt{\frac{1}{M_c}\sum_{m_c=1}^{M_c}\left(\hat{\zeta}_{k,m_c} - \zeta_k\right)^2} \tag{43a}$$

where K is the number of targets, M_c is the number of Monte Carlo trials, ζ_{k,m_c} is the estimate of ζ_k in the m_cth Monte Carlo trial. As in [2], to simplify the RMSE results, we only display the average RMSE of the direction angle estimation (marked as RMSE performance of DAE), namely 2D-DOA and 2D-DOD, and the average RMSE of the polarization parameters estimation (marked as RMSE performance of PAE), namely 2D-TPA and 2D-RPA. A PC (with Interl(R) i7-10750H CPU, 64G RAM) and MATLAB R2020a are used to run the simulation.

First, the proposed parameter estimation approach was applied to the signal subspaces obtained by the PM in [20], EVD in [17], and HOSVD in [18] to prove that the proposed parameter estimation approach can improve parameter estimation accuracy compared with the original parameter estimation approach. Fig.1 (a) and (b) depict the RMSE performance of different

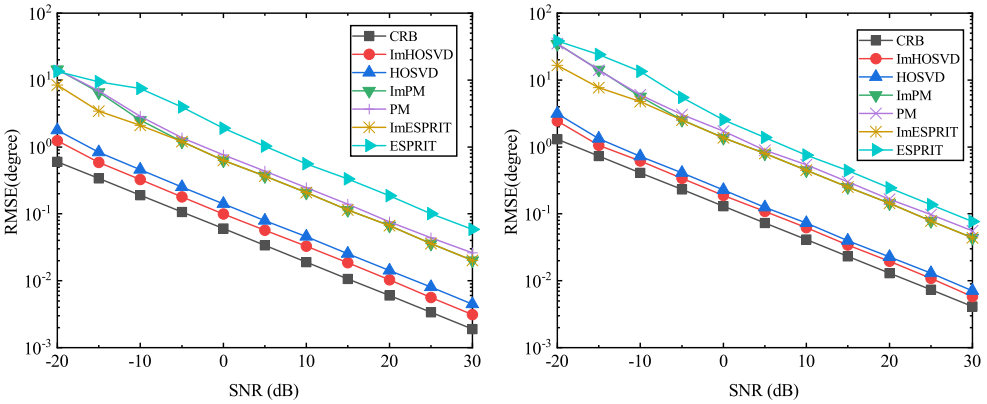

Figure 1: RMSE performance comparison. (a) RMSE performance of DAE. (b) RMSE performance of PAE.

algorithms to estimate the direction angle and polarization parameters, respectively. As shown in Fig.1, whether it is the direction angle estimation or the polarization parameters estimation, the RMSE performance of the proposed approach is better than that of the corresponding traditional parameter estimation approach. This improvement may can from the truth that the proposed approach uses the $36NM$ rows instead of $6N/6M$ rows of the signal subspace to estimate all parameters.

In the following simulations, the average running time (ART) is used to compare the computational complexity of each algorithm. The proposed ImESPRIT-D algorithm, the proposed ImHOSVD-D algorithm, the PM algorithm in [20], the ESPRIT algorithm in [17], the HOSVD algorithm in [18], and the PARAFAC algorithm in [21] are tested from three aspects: the RMSE performance, the average running time (ART), the probability of successfully detecting the target (PSD), thus to show that the proposed ImESPRIT-D and the ImHOSVD-D algorithms have a slight computational complexity and a better parameter estimation performance. Suppose that target can be successfully detected as long as the absolute error of the estimated angle is under ρ_e.

Fig.2 depicts the performance of different algorithms versus SNR, where $L = 100$ and $\rho_e = 1°$. Fig.2 (a)-(b) show that the RMSE performance of different algorithms gradually improves as the SNR increases. The proposed ImHOSVD-D algorithm has the best RMSE performance over other

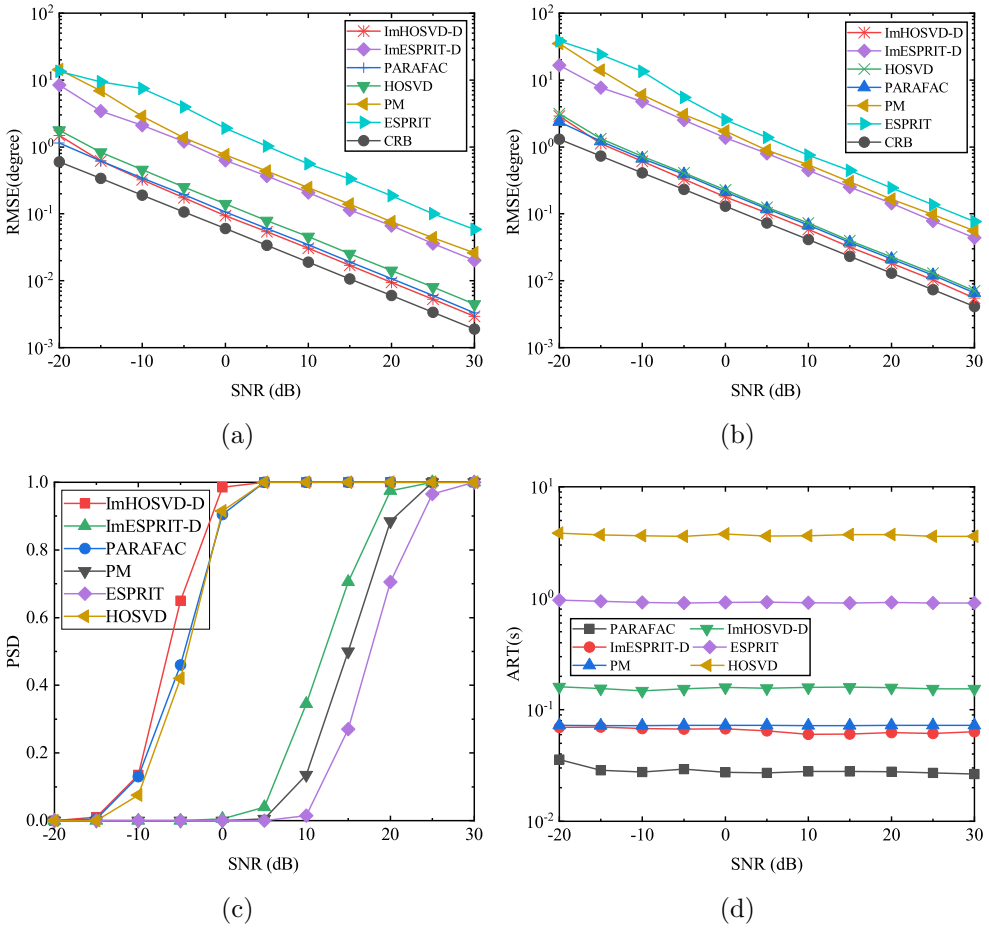

Figure 2: Performance versus SNR. (a) RMSE performance of DAE versus SNR. (b) RMSE performance of PAE versus SNR. (d) PSD versus SNR. (d) ART versus SNR.

algorithms, and the proposed ImESPRIT-D algorithm has a better RMSE performance than the PM and ESPRIT algorithms. The reason has been explained in the first simulation. The proposed ImHOSVD-D algorithm has the best PSD performance, and the ImESPRIT-D algorithm has a better PSD performance than the PM, the ESPRIT algorithms, as shown in Fig.2 (c). From Fig.2 (d), we know that the ART of the proposed ImESPRIT-D algorithm is much shorter than that of the ESPRIT algorithm, and the ART of the proposed ImHOSVD-D algorithm is also much shorter than that of the HOSVD algorithms, even shorter than that of the ESPRIT algorithm.

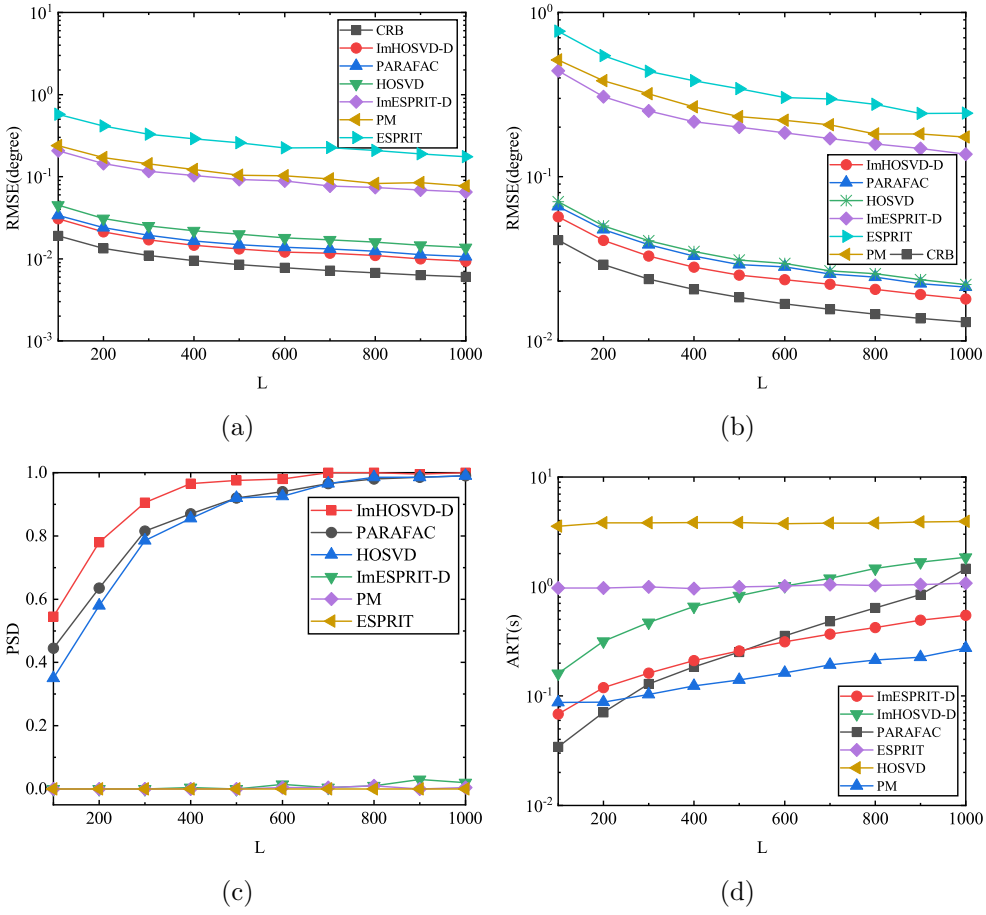

Figure 3: Performance versus L. (a) RMSE performance of DAE versus L. (b) RMSE performance of PAE versus L. (d) PSD versus L. (d) ART versus L.

It can be concluded from Fig.2 that the computational complexity of performing SVD/HOSVD on the data matrix/tensor is much lower than that of performing EVD/HOSVD on the covariance matrix/tensor, which is consistent with the theoretical analysis result of computational complexity. So that when the proposed parameter estimation approach is applied to the two signal subspaces obtained by the proposed methods, the new algorithms can save computation load and provide a better estimation performance at the same time.

Fig.3 depicts the performance of different algorithms versus L, where SNR= 10dB and $\rho_e = 0.15°$. The same conclusion as the second test can

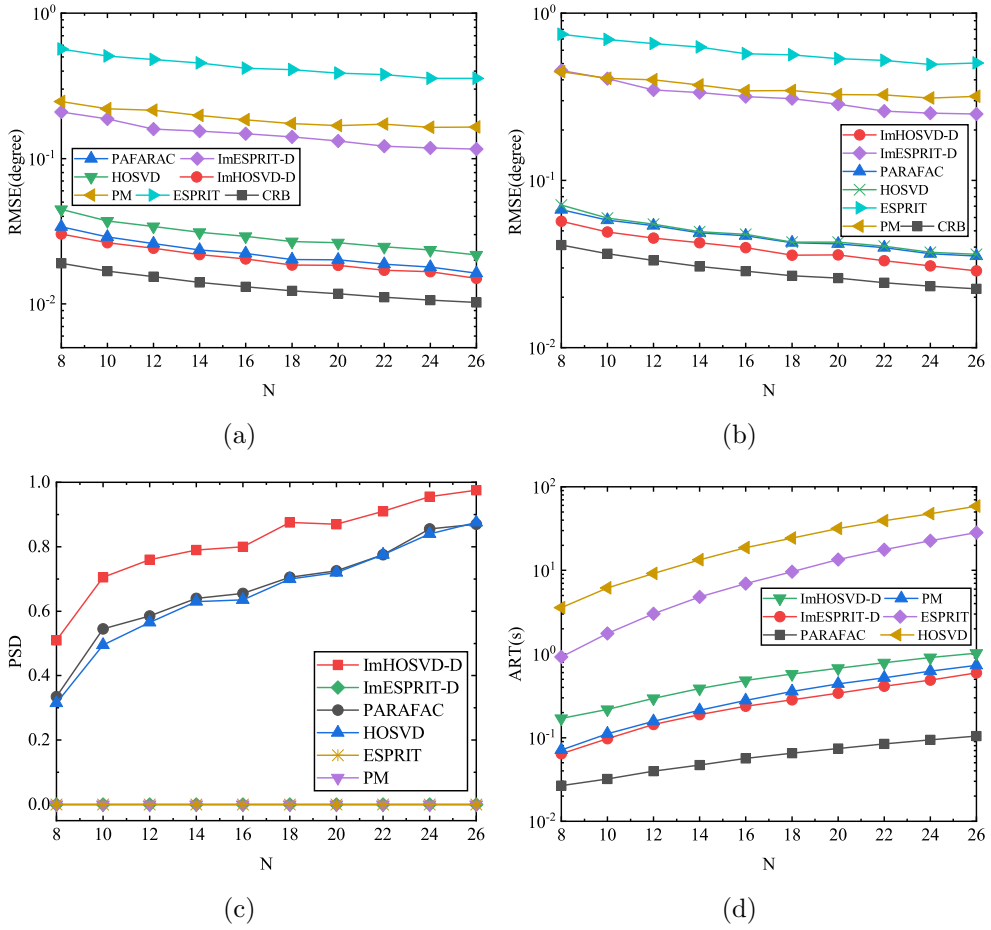

Figure 4: Performance versus N. (a) RMSE performance of DAE versus N. (b) RMSE performance of PAE versus N. (c) PSD versus N. (d) ART versus N.

be drawn from Fig.3(a)-(c) that the proposed ImHOSVD-D algorithm has the best RMSE and PSD performance and the proposed ImESPRIT-D algorithm has a better RMSE performance than the PM and ESPRIT algorithms. The ART of the HOSVD and ESPRIT algorithms is basically unchanged, as shown in Fig.3(d). Because the most time-consuming process of these two algorithms is EVD and high-order SVD, increasing L will not increase the order of the covariance matrix, so their ART does not change much with the increase in L. Besides, the proposed ImHOSVD-D algorithm is more economical than the HOSVD algorithm, and the proposed ImESPRIT-D algorithm

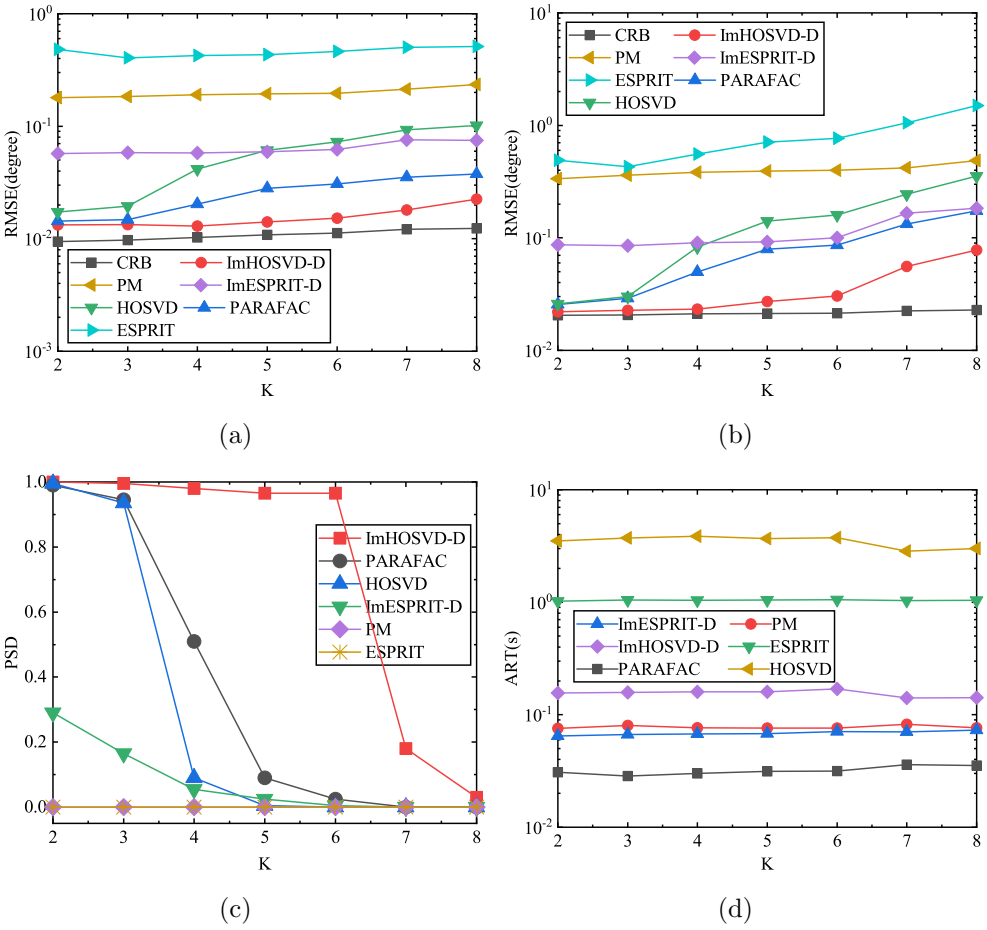

Figure 5: Performance versus K. (a) RMSE performance of DAE versus K. (b) RMSE performance of PAE versus K. (c) PSD versus K. (d) ART versus K.

is also more economical than the ESPRIT algorithm.

Fig.4 depicts the performance of different algorithms versus N, where SNR= 10dB, $L = 100$, and $\rho_e = 0.15°$. The RMSE performance of different algorithms improves less as N increases, as shown in Fig.1(a)-(b). The ART of different algorithms gradually increases as the increase of N. Similarly, the proposed ImHOSVD-D algorithm has the best RMSE and PSD performance and is more economical than the HOSVD; the proposed ImESPRIT-D algorithm is more economical and has a better RMSE performance than the ESPRIT and PM algorithms.

Fig.5 displays the performance of different algorithms versus K, where SNR= 10dB, $L = 100$, and $\rho_e = 0.15°$. The targets are selected from the front K targets from the following targets: $\boldsymbol{\theta}_t = (10°, 15°, 25°, 30°, 35°, 50°, 58°, 67°)$, $\boldsymbol{\phi}_t = (30°, 56°, 15°, 36°, 65°, 22°, 40°, 48°)$, $\boldsymbol{\gamma}_t = (14°, 30°, 54°, 62°, 38°, 46°, 22°, 70°)$, $\boldsymbol{\eta}_t = (18°, 64°, 34°, 56°, 48°, 72°, 30°, 40°)$, $\boldsymbol{\theta}_r = (12°, 52°, 27°, 37°, 20°, 40°, 46°, 40°)$ $\boldsymbol{\phi}_r = (62°, 13°, 54°, 28°, 38°, 34°, 46°, 21°)$, $\boldsymbol{\gamma}_r = (35°, 15°, 25°, 65°, 45°, 55°, 5°, 75°)$, $\boldsymbol{\eta}_r = (81°, 31°, 51°, 61°, 45°, 55°, 5°, 75°)$. As shown in Fig.5 (d), the ART of different algorithms hardly increases with the increase in K. Similar to the previous result, the proposed ImHOSVD-D algorithm has the best RMSE and PSD performance and a shorter ART than that of the HOSVD algorithm; the proposed ImESPRIT-D algorithm has a better RMSE performance and a shorter ART than that of the PM and ESPRIT algorithms. Besides, the proposed ImESPRIT-D algorithm also has a better PSD performance than the PM and ESPRIT algorithms when $K < 6$.

7. Conclusion

In this paper, two economical methods to obtain signal subspace and a more accurate approach for parameter estimation based on signal subspace are introduced for joint 2D-DOD, 2D-DOA, and polarization parameters estimation without pairing. When the improved parameter estimation approach is applied to the signal subspace obtained by performing EVD/HOSVD on the covariance matrix/ tensor or the PM algorithm, the estimation performance can be improved compared with the existing estimation methods. When the parameter estimation approach is applied to the signal subspace obtained by the proposed two methods, the new algorithms can get more accurate estimation results and save computational load.

8. Declarations

Ethical Approval: It is not applicable for both human and animal studies.

Competing interests: No competing interests.

Authors contributions: Fengtao Xue proposed the method, did the simulation, and wrote the paper. Yunxiu Yang, Maoyuan Feng, and Qin Shu check the paper.

Funding: No funding.

Availability of data and materials: the authors have the corresponding simulation data.

References

[1] E. Fishler, A. Haimovich, R. Blum, D. Chizhik, L. Cimini, R. Valenzuela, Mimo radar: an idea whose time has come, in: Proceedings of the 2004 IEEE Radar Conference (IEEE Cat. No.04CH37509), 2004, pp. 71–78.

[2] J. Li, P. Stoica, Mimo radar with colocated antennas, IEEE Signal Processing Magazine 24 (5) (2007) 106–114.

[3] A. M. Haimovich, R. S. Blum, L. J. Cimini, Mimo radar with widely separated antennas, IEEE Signal Processing Magazine 25 (1) (2007) 116–129.

[4] R. Xie, Z. Liu, Z. J. Zhang, Doa estimation for monostatic mimo radar using polynomial rooting, Signal Processing 90 (12) (2010) 3284–3288.

[5] W. Wang, X. Wang, H. Song, Y. Ma, Conjugate esprit for doa estimation in monostatic mimo radar, Signal Processing 93 (7) (2013) 2070–2075.

[6] M. L. Bencheikh, Y. Wang, H. He, Polynomial root finding technique for joint doa dod estimation in bistatic mimo radar, Signal Processing 90 (9) (2010) 2723–2730.

[7] Y. Cheng, R. Yu, H. Gu, W. Su, Multi-svd based subspace estimation to improve angle estimation accuracy in bistatic mimo radar, Signal Processing 93 (7) (2013) 2003–2009.

[8] Zhao, Yongbo, Li, Hui, Cheng, Zengfei, Xu, Baoqing, A novel unitary parafac method for dod and doa estimation in bistatic mimo radar, Signal Processing: The Official Publication of the European Association for Signal Processing (EURASIP) (2017).

[9] C. Chen, X. Zhang, A low-complexity joint 2d-dod and 2d-doa estimation algorithm for mimo radar with arbitrary arrays, International Journal of Electronics 100 (10-12) (2013) 1455–1469.

[10] J. Li, X. Zhang, Closed-form blind 2d-dod and 2d-doa estimation for mimo radar with arbitrary arrays, Wireless Personal Communications 69 (1) (2013) 175–186.

[11] T. Xia, Joint diagonalization based 2d-dod and 2d-doa estimation for bistatic mimo radar, Signal Processing 116 (2015) (2015) 7–12.

[12] K. T. Wong, M. D. Zoltowski, Uni-vector-sensor esprit for multisource azimuth, elevation, and polarization estimation, Antennas & Propagation IEEE Transactions on 45 (10) (1997) 1467–1474.

[13] K. T. Wong, X. Yuan, "vector cross-product direction-finding" with an electromagnetic vector-sensor of six orthogonally oriented but spatially noncollocating dipoles/loops, IEEE Transactions on Signal Processing 59 (1) (2010) 160–171.

[14] X. Yuan, Estimating the doa and the polarization of a polynomial-phase signal using a single polarized vector-sensor, IEEE Transactions on Signal Processing 60 (3) (2012) 1270–1282.

[15] C. Gu, J. He, H. Li, X. Zhu, Target localization using mimo electromagnetic vector array systems, Signal Processing 93 (7) (2013) 2103–2107.

[16] Yuan, X., Coherent sources direction finding and polarization estimation with various compositions of spatially spread polarized antenna arrays, Signal Processing Amsterdam (2014).

[17] Chintagunta, Srinivasarao, Ponnusamy, Palanisamy, 2d-dod and 2d-doa estimation using the electromagnetic vector sensors, Signal Processing the Official Publication of the European Association for Signal Processing (2018).

[18] C. Mao, J. Shi, F. Wen, Target localization in bistatic emvs-mimo radar using tensor subspace method, IEEE Access 7 (2019) 163119–163127.

[19] T. Liu, F. Wen, J. Shi, Z. Gong, H. Xu, A computationally economic location algorithm for bistatic evms-mimo radar, IEEE Access 7 (2019) 120533–120540.

[20] F. Wen, J. Shi, Fast direction finding for bistatic emvs-mimo radar without pairing, Signal Processing 173 (2020) 107512.

[21] F. Wen, J. Shi, Z. Zhang, Joint 2d-dod, 2d-doa and polarization angles estimation for bistatic emvs-mimo radar via parafac analysis, IEEE Transactions on Vehicular Technology PP (99) (2019) 1–1.

[22] T. G. Kolda, B. W. Bader, Tensor decompositions and applications, Siam Review 51 (3) (2009) 455–500.